Biophysical Chemistry 158 (2011) 96–103

Contents lists available at ScienceDirect

Biophysical Chemistry

journal homepage: http://www.elsevier.com/locate/biophyschem

Resolution of localized small molecule–Aβ interactions by deep-ultraviolet resonance Raman spectroscopy

Mingjuan Wang [1], Renee D. JiJi *

Department of Chemistry, University of Missouri, Columbia, MO 65211, USA

ARTICLE INFO

Article history:
Received 13 April 2011
Received in revised form 19 May 2011
Accepted 19 May 2011
Available online 27 May 2011

Keywords:
Alzheimer's disease
Amyloid-β peptide
Ultraviolet resonance Raman
Circular dichroism
Thioflavin T
Myricetin

ABSTRACT

The mechanism by which flavonoids prevent formation of amyloid-β (Aβ) fibrils, as well as how they associate with non-fibrillar Aβ is still unclear. Fresh, un-oxidized myricetin exhibited excitation and emission fluorescence maxima at 481 and 531 nm, respectively. Introduction of either Aβ(1–42) or Aβ(25–40) resulted in a fluorescence decrease, when measured at 481 nm, suggesting formation of a myricetin–Aβ complex. Circular dichroism (CD) and ultraviolet resonance Raman (UVRR) studies indicate that the association of myricetin with the Aβ peptide or its hydrophobic fragment, Aβ(25–40), leads to subtle changes in each peptide's conformation. Aβ(25–40) formed amyloid fibrils at a similar rate, when compared to the full-length peptide, Aβ(1–42), using thioflavin T (ThT) fluorescence. Studies also indicated that myricetin was equally effective at preventing the formation of both Aβ(1–42) and Aβ(25–40) fibrils. Although ThT assays indicated that Aβ(1–16) did not form amyloid fibrils, CD studies of the hydrophilic fragment, Aβ(1–16), suggest possible interactions between myricetin and aromatic side chains. UVRR studies of the full-length peptide and Aβ(1–16) showed increases in the intensity of the aromatic modes upon introduction of myricetin. Our findings suggest that myricetin interacts with soluble Aβ via two mechanisms, association with the hydrophobic C-terminal region and interactions with the aromatic side chains.

© 2011 Elsevier B.V. All rights reserved.

1. Introduction

Alzheimer's disease (AD) is characterized by two pathological hallmarks: senile plaques and neurofibrillary tangles. Senile plaques are insoluble extracellular accumulations of the amyloid-β peptide (Aβ), which is typically 39–43 residues in length. In contrast neurofibrillary tangles are intracellular fibrillar accumulations of the tau protein [1]. However, it was found that the level of soluble Aβ was correlated to the severity of neurodegeneration in AD, rather than the abundance of amyloid plaques [2,3]. Clinical symptoms of AD initially include difficulty with memory, progressive confusion, disorientation, impaired expression, and progressive loss of mobility [4].

Current therapies primarily involve cholinesterase inhibitors [5] or the *N*-methyl-D-aspartate receptor modulator memantine [6], which reduce symptoms but do not prevent the advancement of AD. Prospective therapeutic strategies aimed at halting, reversing or preventing AD target either Aβ or tau protein. Currently, the predominance of research focuses on decreasing the production of Aβ from the amyloid precursor protein (APP) by inhibiting or modulating the APP proteolytic cleavage enzymes: β-secretase [7], γ-secretase [8] and α-secretase [9]. Alternative strategies entail clearance of existing Aβ plaques through active and passive immunization against Aβ. Active immunization with vaccine AN-1792 in PDAPP transgenic mice has been shown to prevent plaque formation and improve cognition [10]. However, the first clinical trial was halted because 6% of vaccinated patients developed meningoencephalitis [11]. Passive immunization with the humanized monoclonal antibody bapineuzumab (AAB-001) has completed phase II clinical trials [12] and has been shown to reduce fibrillar Aβ in the cerebral cortex of AD patients [13]. Although immunotherapy is a promising strategy, there is a lack of consensus on the mechanism involved in reduction of Aβ deposition [14].

While immunotherapy is a promising treatment for AD, there are no forthcoming preventative strategies. However, there is evidence that long-term adherence to a diet rich in plant derived foods is associated with a reduced risk of AD [15]. In addition, plant derived products or extracts have been shown to have neuroprotective properties [16–19], which are thought to be derived from the abundant polyphenolic compounds found in these products. Thus, investigation into the neuroprotective activity of small organic molecules has expanded dramatically. Numerous naturally occurring, small molecules have been identified that inhibit the formation of amyloid fibrils or disaggregate them [20–25]. Furthermore, many of these compounds significantly decrease the toxicity of Aβ in vitro, including selected inositol stereoisomers [26], curcumin [19], resveratrol [27], melatonin [28], and rifampicin [29]. What little known is about the

* Corresponding author at: Department of Chemistry, University of Missouri, 601 South College Avenue, Columbia, MO 65211, USA. Tel.: +1 573 882 8949; fax: +1 573 882 2745.
E-mail address: jijir@missouri.edu (R.D. JiJi).
[1] Present address: Rhodia Co. Ltd., 3966 Jin Du Road, Xin Zhuang Industrial Zone, Shanghai 201108, China.

0301-4622/$ – see front matter © 2011 Elsevier B.V. All rights reserved.
doi:10.1016/j.bpc.2011.05.017

mechanisms behind these molecules' anti-amyloidogenic and neuroprotective activity indicate great variety in their modes of action.

Flavonoids have also been shown to reduce the toxicity of Aβ and its fragments in vitro [30,31] and in vivo [32,33]. Flavonoids are polyphenolic antioxidants, which are composed of one or more aromatic phenolic rings [34]. Natural flavonoids are abundant in the roots, seeds, flowers, barks and leaves of a large variety of vegetables and herbs. Beverages, such as wine and tea also contain high amounts of flavonoids [35].

A study of previously identified anti-amyloidogenic small molecules separated these molecules into three classes: (I) compounds that inhibit oligomer formation but do not prevent fibrillogenesis, (II) compounds that inhibit fibrillization but do not interfere with oligomerization, and (III) compounds that inhibit both oligomerization and fibril formation [20]. Myricetin, a flavonoid compound, was categorized as a class I compound. These findings were echoed in a more recent study, which showed that Tg2576 transgenic mice fed myricetin over a 5-month period had reduced levels of A11 anti-oligomeric reactive oligomers but increased plaque burden with respect to controls [36]. However, some in vitro studies have shown that myricetin interferes with Aβ fibril formation and elongation [37], as well as prevents conversion to β-sheet sheet structure during incubation [38].

Currently, it is not known how myricetin interacts with Aβ. However, it has been shown that polyphenols bind disordered proline rich salivary proteins (PRP) with the main binding sites being proline residues [39,40]. One study suggested that sequential proline residues play a role in PRP–polyphenol binding by allowing access to and hydrogen bonding with the peptide backbone [39], while another found secondary hydrogen bonding with positively charged arginine served to stabilize the complex [40]. Along with hydrogen bonding to the peptide backbone or positively charged arginine, hydrophobic interactions were also found to be important for complex formation [39,40]. Although Aβ has no proline residues, the hydrophobic region is glycine rich, with sequential glycines at residues 37 and 38. Thus it is possible that transient interactions between myricetin and monomeric or oligomeric Aβ play a role in the reduction of Aβ oligomers. A better understanding of the interactions between small molecules and Aβ may help to clarify the mechanism underlying Aβ aggregation and may shed light on the therapeutic properties of small molecules. Furthermore, a better understanding of these interactions would be useful in the design of new small molecule based therapies for AD.

In this work, we report the use of various spectroscopic methods to identify potential binding interactions between Aβ and myricetin. Tandem experiments using circular dichroism (CD) and thioflavin T (ThT) fluorescence assay suggests that myricetin does inhibit amyloid formation of the hydrophobic fragment, Aβ(25–40), as well as Aβ(1–42). Furthermore, CD and ultraviolet resonance Raman (UVRR) studies indicate that myricetin induces a small but immediate (within the timeframe of the experiments) conformational change in both Aβ(25–40) and Aβ(1–42), suggesting that hydrophobic or backbone interactions may contribute to Aβ-flavonoid binding. In addition, both CD and UVRR studies indicate changes in the environment surrounding one or more aromatic residues upon introduction of myricetin, suggesting aromatic interactions may be another factor in flavonoid binding to Aβ.

2. Experimental procedures

2.1. Materials

Aβ(1–42), Aβ(25–40) and Aβ(1–16) were purchased from Global Peptide (Fort Collins, CO) and used without further purification (96% purity). The phosphate buffer was made from sodium phosphate monobasic and sodium phosphate dibasic, both of which were purchased from Fisher Scientific (Pittsburgh, PA). Ammonium hydroxide was also purchased from Fisher Scientific. Sodium perchlorate was purchased from Sigma-Aldrich (Acros Organics, Geel, Belgium). Myricetin was purchased from Sigma-Aldrich (Saint Louis, MO).

2.2. Sample preparation

Aβ(1–42) (M.W. 4511) and the fragment peptides, Aβ(1–16) (M.W.1954) and Aβ(25–40) (M.W. 1472), were dissolved in 0.1 M ammonium hydroxide. Previous studies have shown that presolubilization at high pH increases the final concentration of monomers and dimers, termed low molecular weight (LMW) peptide [41]. When necessary a small amount of 1 M ammonium hydroxide was added to bring the final pH up to 10.5. The resultant solutions were then sonicated in an ice bath for 2 min to break up aggregates. The solutions were then lyophilized and re-suspended into 10 mM sodium phosphate buffer for a final pH of 7.4 and sonicated to further break up any remaining aggregates. Then, the solution was centrifuged for 30 min at 14,000 rcf, with a 10 kDa molecular weight cutoff (MWCO) filter (Fisher Scientific, Pittsburgh, PA) to remove aggregates greater than dimers for full-length Aβ or greater than heptamers for Aβ fragments. The concentrations of Aβ(1–42) and Aβ(1–16) in the filtrates were estimated from tyrosine extinction coefficient at 280 nm (1280 $M^{-1}cm^{-1}$). The molar extinction coefficient of Aβ(25–40) at 215 nm was estimated as 17,385 $M^{-1}cm^{-1}$ from side chain and peptide bond extinction coefficients at 215 nm [42].

2.3. Fluorescence measurements

A Cary Eclipse fluorescence spectrometer (Varian, Palo Alto, CA) was used to collect fluorescence spectra. A 3 mm optical path length quartz cell (Hellma USA, Plainview, NY) was used for all fluorescence experiments.

2.3.1. Thioflavin T (ThT) assay

Solutions of Aβ(1–42) and its fragments, Aβ(25–40) and Aβ(1–16), were prepared as stated. Each sample was then divided into two equal volume samples. Concentrated myricetin dissolved in ethanol was then added to one of the samples. The final concentration of myricetin was 25 μM. Samples were then incubated at 37 °C for 10 days. During the incubation period, 65 μL aliquots were removed from the samples to test for amyloid formation. A small volume of concentrated ThT in 10 mM phosphate buffer was added to each sample to a final concentration of 5 μM ThT. The excitation wavelength was set to 450 nm and emission spectra were generated between 470 and 600 nm. The fluorescence intensity at 480 nm versus the number of days incubated was plotted.

2.3.2. Intrinsic fluorescence of myricetin

Solutions of Aβ(1–42) and its fragments, Aβ(25–40) and Aβ(1–16), were prepared as stated above. Each sample was diluted with 10 mM phosphate buffer solution at pH 7.4 for a final peptide concentration of 30 μM and divided into two equal samples. Concentrated myricetin dissolved in ethanol was then added to one peptide sample for a final myricetin concentration of 10 μM. The excitation and emission resolutions were set to 10 nm. The excitation wavelength was set at 380 nm and the emission spectra were generated between 450 and 600 nm.

2.4. Circular dichroism (CD)

CD spectra were obtained using an AVIV 62DS Circular Dichroism Spectrometer (Aviv, Lakewood, NJ). A quartz cell with 1 mm optical path length was used (Hellma USA, Plainview, NY). The spectral range was 190–250 nm with a resolution of 0.1 nm and bandwidth of 1 nm. A scan speed of 1 nm/5 s was employed and 5 scans were measured for each. The background spectrum was subtracted and the results were expressed as mean residue molar ellipticity [θ_{MRE}]:

$$[\theta_{MRE}] = \frac{\theta * MRW}{10 * d * c} \quad (1)$$

where θ is the raw ellipticity from the measurement; MRW is the mean residue weight, which is equal to molecular weight/number of residues; d is the path length (cm) of the cell and c is the concentration in g/mL (g/cm^3).

2.5. Ultraviolet resonance Raman (UVRR) spectroscopy

UVRR spectra were obtained using the fourth harmonic of a 4 kHz frequency quadrupled Ti:Sapphire laser (Coherent Inc., Santa Clara, CA), tunable from 193 to 210 nm. The Ti:Sapphire laser was pumped using a diode-pumped frequency doubled Nd:YLF laser (Coherent Inc., Santa Clara, CA). Samples were excited at 200 nm; the average power at the sample was approximately 0.5 mW To prevent degradation.

Samples were held in a custom-made water-jacketed reservoir (Mid Rivers Glassblowing, Saint Charles, MO) of in-house design and circulated using a model 75211–10 gear pump (Cole Palmer, Vernon Hills, Illinois). Samples were maintained at ~7 °C using a Isotemp 3016D circulating water bath (Fisher Scientific, Pittsburgh, PA). A wire-guided stream of sample was held within a temperature controlled sample chamber, of in-house design, with a steady stream of nitrogen gas flowing over the sample to remove ambient oxygen. The Raman scattering was collected in the 135° backscattering geometry and dispersed using a 1.25 m spectrometer (Horiba Jobin Yvon Inc., Edison, NJ) fitted with 3600 groove/mm grating. The spectrometer was equipped with a back illuminated, phosphor coated, liquid nitrogen cooled Symphony CCD camera (Horiba Jobin Yvon Inc., Edison, NJ) with a chip size of 2048×512 pixels. The maximum resolution of the instrument was approximately 0.6 cm^{-1}. Pixels were binned in the horizontal direction in increments of four, for a final resolution of approximately 2.4 cm^{-1}. Spectra were collected and exported using Synergy software (Horiba Jobin Yvon Inc., Edison, NJ).

Spectra were calibrated using a standard cyclohexane spectrum. Each sample contained 50 mM sodium perchlorate (ClO_4^-, 932 cm^{-1}), which was used as an internal intensity standard.

2.6. Data analysis

All spectra were analyzed in the Matlab (Mathworks, Natick, MA) environment. UVRR and fluorescence spectra were deconvoluted into a series of Gaussian/Lorentzian bands, which approximate the more computationally intensive Voight line shape, using the nonlinear least-squares (NLLS) algorithm with a program written in-house for the Matlab environment.

3. Results

3.1. ThT assays for amyloid structures

Previous studies have shown that myricetin inhibits the formation of amyloid fibrils from full-length Aβ [30]. A ThT assay was used to characterize the propensity of Aβ and its fragments to form amyloid structures and myricetin's ability to inhibit amyloid formation. As described earlier, fresh samples of Aβ and its fragments were prepared and divided into two samples, one of which was then treated with myricetin at a final concentration of 25 μM. Aβ(1–16) failed to show significant amyloid formation within the time frame of these experiments (data not shown).

ThT fluorescence assays indicated that Aβ(1–42) formed amyloid or cross β-sheet structure within 8 days (Fig. 1A). The peptide sample treated with myricetin exhibited no increase in ThT fluorescence during the course of the experiment. Similar results were observed for Aβ(25–40) (Fig. 1B), indicating that Aβ(25–40) is amyloidogenic. Some small molecules interfere with ThT binding [20]; therefore, CD spectra were collected over the course of 2 weeks to monitor any structural changes. The CD results shown in Fig. 2A indicate that myricetin inhibited Aβ(1–42) from forming β-sheet structure over the course of the experiment. The control sample formed β-sheet structure within 7 days (Fig. 2B). Interestingly, the magnitude of the minima observed at 197 nm appears to decrease over the 2-week period, perhaps indicating alternate changes in secondary structure, such as a loss of poly-proline II (PPII) structure. PPII structure is a non-random extended helical structure initially observed in poly-proline [43] and later in other unfolded peptides [44,45]. The loss of PPII in favor of more amorphous structure could account for these spectral changes [46,47].

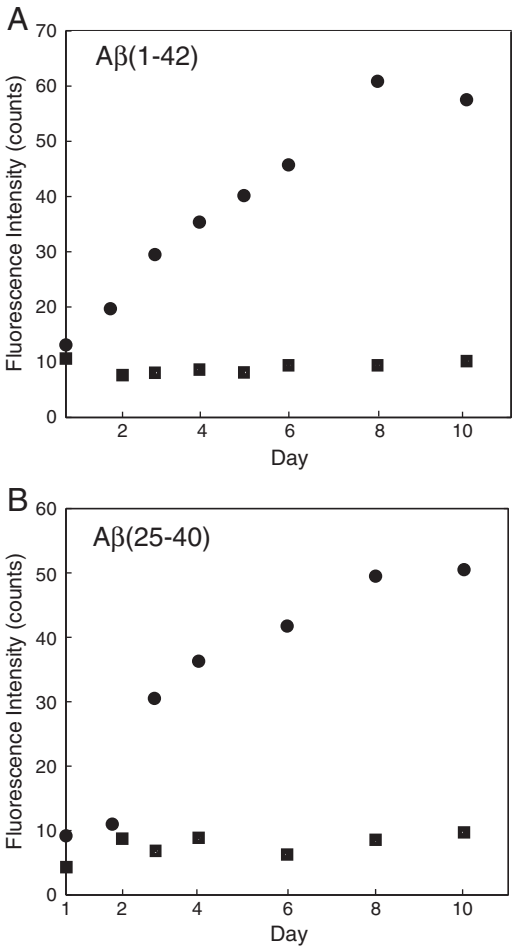

Fig. 1. ThT fluorescence (λ_{em} = 480 cm), in the presence of ~125 μM Aβ(1–42) (A) or Aβ(25–40) (B) after incubation at 37 °C in the absence (●) or presence (■) of 25 μM myricetin.

3.2. Circular dichroism (CD)

Fresh samples of Aβ(1–42), Aβ(25–40) and Aβ(1–16) were prepared as described in the preceding section. Each peptide sample was then divided into two equal samples, one of which was spiked with myricetin, at final concentration of 25 μM. The difference in peptide concentration due to the additional volume (2 μL) of myricetin stock solution added was assumed to be negligible. The CD spectrum of Aβ(1–16) (Fig. 3) has a strong negative feature at 197 nm and a positive feature at 220 nm, consistent with a significant proportion of PPII content [45]. The negative feature at 197 nm for Aβ(25–40) sample (Fig. 3) was less intense with respect to Aβ(1–16), suggesting a decreased proportion of PPII content. This is consistent with previous studies that found that the hydrophobic region contained a mixture of amorphous (coil) and β-strand structures [48]. Interestingly, the CD spectrum of Aβ(25–40) had another weak negative feature around 220 nm. A very small fraction of β-sheet

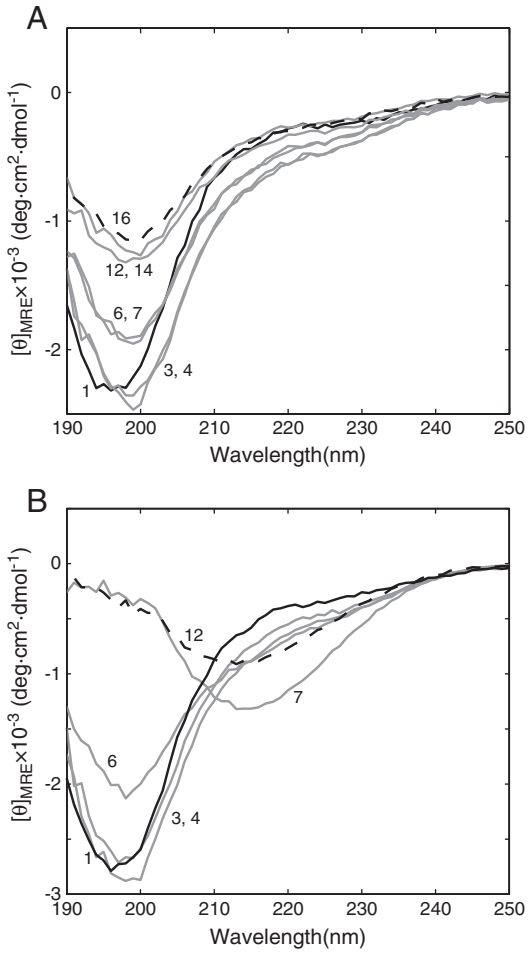

Fig. 2. CD spectra of Aβ(1–42) during the (A)16 day incubation at 37 °C with 25 μM myricetin and (B)12 day incubation at 37 °C. Initial CD spectra are shown in black (—), intermediate spectra are shown in gray (—) and the final spectra are shown in black dashed lines (— —).

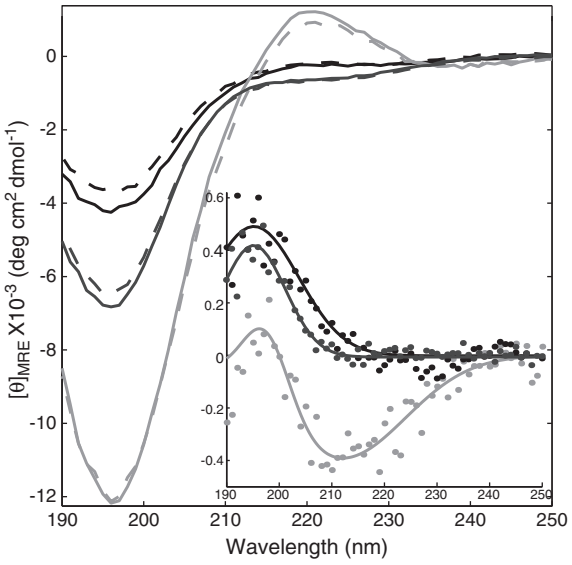

Fig. 3. CD spectra of Aβ(1–42) (—), Aβ(25–40) (—) and Aβ(1–16) (—) at pH 7.4, 4 °C, with (dashed lines) and without myricetin. The inset shows the difference spectra for Aβ with myricetin—Aβ, Aβ(1–42) (—), Aβ(25–40) (—) and Aβ(1–16) (—).

structure could account for this small minimum at approximately 220 nm. The CD spectrum of Aβ(1–42) (Fig. 3) has no positive feature at 220 nm and the least intense negative feature at ~197 nm in comparison to Aβ(1–16) and Aβ(25–40). A subtle change in the molar ellipticity at 197 nm was observed for Aβ(1–42) and Aβ(25–40) in solutions containing myricetin (Fig. 3). Difference spectra show a single positive feature at approximately 197 nm for both peptides (Fig. 3, inset). This suggests that a small change in the secondary structure of the bulk peptide population is occurring upon introduction of myricetin. Alternatively, a small fraction of the peptide population could be undergoing a larger scale structural change; however, this scenario is less likely. In contrast, the change at 197 nm was not significant upon introduction of myricetin to samples containing the hydrophilic fragment Aβ(1–16) (Fig. 3), though a significant change was observed in the region from 210 to 220 nm for Aβ(1–16). No change was seen in this region with Aβ(1–42) or Aβ(25–40). Previous studies show that aromatic side chains make evident contributions to CD spectra in this region. The phenylalanine side chain contributes to optical activities at 210 nm, as well as 185 and 255 nm [49]. This contribution increases in proportion to the phenylalanine content of the peptide. Changes in the environment of phenylalanine can induce CD spectral changes at 210 nm, even if there is no conformational change in the homo-polypeptide backbone structure [49]. Another study showed that tyrosine contributes a broad positive band centered at 221 nm in deep-UV CD spectra of helical proteins [50]. Thus, the CD spectrum of Aβ(1–16) treated with myricetin suggests the possibility of interactions between myricetin and the tyrosine (Y10) or phenylalanine (F4) residues. It is not clear why similar spectral differences were not observed for Aβ(1–42) treated with myricetin; however, the lower relative proportion of tyrosine (1 out of 42 residues), as compared to Aβ(1–16), may be a factor, which will be discussed in the next section.

3.3. UVRR spectroscopy

3.3.1. Assignments of amide and aromatic bands

UVRR spectra of proteins have four structurally sensitive regions, the amide I (1600–1690 cm^{-1}), II (1450–1580 cm^{-1}), III (1200–1300 cm^{-1}) and S (1300–1425 cm^{-1}) regions [51–53]. The main contribution of the amide I band is the in-plane C = O stretching mode. Hydrogen bonding will shift the amide I band, because of the concomitant decrease in the double bond character of the C = O bond and increase in the C-N bond order [54]. The amide II and III modes are mainly the out-of-phase and in-phase combinations of C-N stretching and N-H in-plane bending, respectively. The amide S mode is a C_α-H bending mode, which is resonance enhanced in β-sheet and disordered polypeptides due to the coupling of the N-H and C_α-H bending vibrations [54].

3.3.2. Aβ(1–42)

Aβ(1–42) is a fully disordered peptide [48,55]. UVRR has been employed previously to characterize the core structure in Aβ(1–40) fibrils [56], as well as the fibrillization of other amyloidogenic peptides and proteins [57–61]. The UVRR spectrum of LMW Aβ(1–42) is visually similar to other disordered homo-polypeptides (Fig. 4A), including poly(L-lysine) at low pH values and poly(L-glutamic acid) at high pH [51,53,62,63]. The amide I band could be fit with single peak centered at 1667 cm^{-1}. The amide II band could be fitted with two peaks centered at 1525 and 1556 cm^{-1}, respectively. Multivariate studies using a series of well characterized globular proteins indicate that the amide I band should occur at approximately 1665 cm^{-1} for disordered structures [51,64]. However, there is less agreement with respect to the position of the amide II band, which was predicted to occur at 1560 cm^{-1} in one study [51], and almost 10 cm^{-1} lower at 1552 cm^{-1} in another study [64]. There is similar variability in the observed position of the amide II band in disordered homo-polypeptides [51,53,62–64].

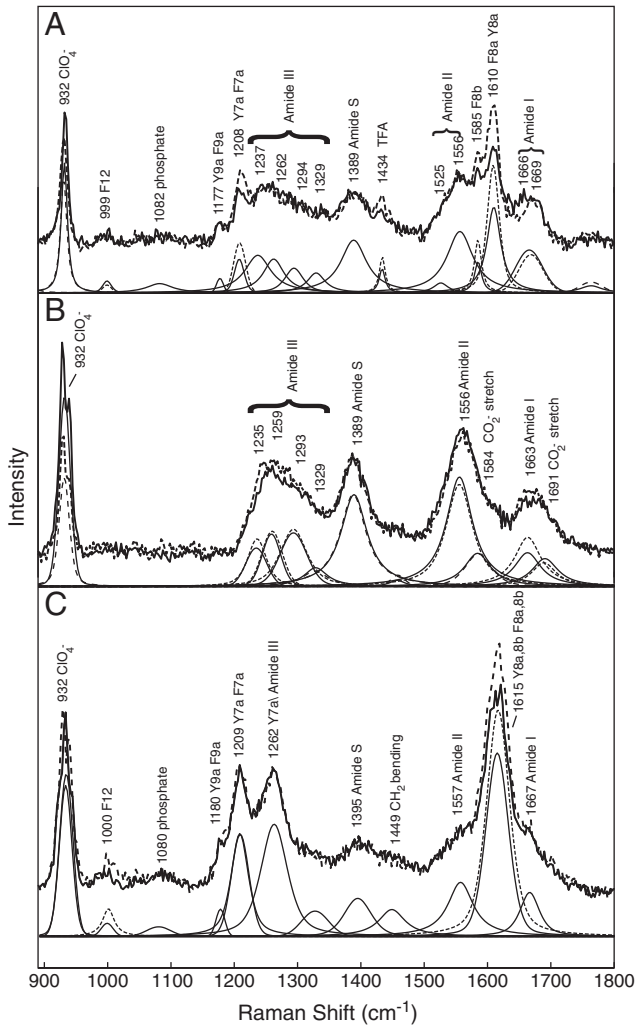

Fig. 4. UVRR spectra of (A) Aβ(1–42), (B) Aβ(25–40) and (C) Aβ(1–16) with (– – –) and without (—) 25 μM myricetin in pH 7.4 phosphate buffer (λ_{Ex} = 200 nm), including raw spectra (top) and the fitted peaks (below).

Disordered peptides contain both PPII and β-strand structures. Previous UVRR studies have indentified discrete amide III bands associated with PPII and β-strand structures [53,64,65]. The amide III region of the UVRR spectrum of Aβ(1–42) was deconvoluted into four components centered at 1237, 1262, 1294 and 1329 cm^{-1}. Although the fitted positions are 5–10 cm^{-1} lower than previous studies [65], the lowest frequency components at 1237 and 1262 cm^{-1} are likely associated with PPII and β-strand structures, respectively. The position of these bands is dependent upon the peptide backbone secondary structure [51,53,62–64] and exhibits a sinusoidal dependence on the ψ dihedral angle [66,67]. The component at 1294 cm^{-1} is similar in position to a band observed for poly(L-lysine) that has been assigned to PPII structure [65]. The amide S (C_α-H b) band in disordered homopolypeptides is typically asymmetrical with two underling components in the ranges of 1369–1380 and 1396–1399 cm^{-1}[53,65]. However, a single component, midway between the two ranges noted above, at 1389 cm^{-1} was sufficient to model the amide S band of Aβ(1–42); the observed amide S band could be a composite of two underlying amide S bands.

Rava and Spiro characterized the UVRR spectra of phenylalanine, tyrosine and tryptophan [68]. Since Aβ(1–42) contains no tryptophan, only tyrosine and phenylalanine features will be addressed here. The majority of the phenylalanine vibrational modes are derived from the monoalkylbenzene. The ring C–C stretching modes at 1606 (ν_{8a}), 1586 (ν_{8b}) and 1000 cm^{-1} (ν_{12}) are sensitive to the polarity of the surrounding environment [69]. The observed band at 1208 cm^{-1} arises from symmetric C_{ring}–C_{ext} stretching (ν_{7a}), while the band at 1177 cm^{-1} (ν_{9a}) arises from C-H bending as well as ring C–C stretching. The ring C–C stretching modes of tyrosine are up-shifted to 1601 and 1617 cm^{-1}. Likewise, the symmetric C_{ring}–C_{ext} stretching mode is at 1210 cm^{-1}, slightly higher than that of phenylalanine. In addition, tyrosine has a C_{ring}–O stretching mode, which occurs at 1263 cm^{-1} ($\nu_{7a'}$) and has been found to be highly sensitive to hydrogen bonding.

Aβ(1–42) has one tyrosine (Y10) and three phenylalanines (F4, F19, F20) residues, which also make strong contributions to the deep UVRR spectra of proteins. The strong peak at 1610 cm^{-1} in the UVRR spectrum of Aβ(1–42) likely arises from unresolved tyrosine and phenylalanine ring C–C stretch vibrational modes (ν_{8a}). The band at 1585 cm^{-1} can be assigned to phenylalanine (ν_{8b}). The peaks at 1177 and 1208 cm^{-1} are also likely combinations of the tyrosine and phenylalanine ν_{7a} and ν_{9a} modes, respectively.

Addition of myricetin results in an up-shift of the amide I band (Fig. 4A), which is shifted from 1666 to 1669 cm^{-1}. However, the amide III bands remain unchanged. This shift in the amide I band may suggest a subtle change in the peptide's secondary structure. Interestingly, the largest change in the Aβ(1–42) spectrum with myricetin is with the aromatic bands at 1610, 1585 and 1208 cm^{-1}. These data suggest that the environment surrounding the phenylalanine and possibly tyrosine residues is changing.

3.3.3. Aβ(25–40)

Aβ(25–40) has no aromatic residues, which greatly simplifies the UVRR spectrum (Fig. 4B). One band was needed to fit the amide I region at 1663 cm^{-1}, which can be assigned to a disordered structure [64]. Another band at 1691 cm^{-1}, close to the amide I band, may arise from the symmetrical CO_2^- stretch of the C-terminal carboxylic acid [70]. Two components were again needed to model the amide II region; the first at 1556 cm^{-1} can be assigned to the amide II band of a disordered protein [51,64]. The higher frequency component at 1584 cm^{-1} may be associated with the asymmetrical CO_2^- stretch, which occurs in the region of 1560–1600 cm^{-1} in free amino acids [70]. Given that Aβ(25–40) is a short peptide and has no aromatic residues, observation of the symmetrical and asymmetrical stretches of the C-terminal carboxylic acid is not surprising. The amide III band region was again deconvoluted into four components at 1235, 1259, 1293 and 1329 cm^{-1}, which are similar in position to those associated with the amide III region of Aβ(1–42). A single component at 1389 cm^{-1} was again sufficient to model the amide S region.

Similar to the CD spectra of Aβ(25–40), addition of myricetin had only a small effect on the UVRR spectrum of Aβ(25–40). The most significant changes were slight increases in the intensities of the amide I and III bands in comparison to the amide S band. Interestingly, the amide III bands at 1235 and 1293 cm^{-1} (PPII) increased in intensity in comparison to the band at 1259 cm^{-1}, suggesting that the addition of myricetin may shift the equilibrium towards PPII structure.

3.3.4. Aβ(1–16)

Aβ(1–16) has one phenylalanine and one tyrosine residue at positions 4 and 10, respectively. The UVRR spectrum of Aβ(1–16) (Fig. 4C) is dominated by the spectral features of the single tyrosine residue. The strong band centered at 1615 cm^{-1} can be assigned to the unresolved ν_{8a} (1617 cm^{-1}) and ν_{8b} (1609 cm^{-1}) ring C–C stretching vibrations of tyrosine. Phenylalanine is also expected to contribute to this band, although to a lesser extent than for the full-length Aβ(1–42) peptide, which has three phenylalanine residues. Characteristic tyrosine bands are also observed at 1180, 1209 and 1262 cm^{-1}. The phenylalanine band at 1000 cm^{-1} is quite weak, suggesting that the relative contribution of phenylalanine to the spectrum is small. The amide bands are also quite weak. The position

of the amide I, II and S bands is 1667, 1557 and 1395 cm^{-1}, respectively, consistent with other disordered peptides. The amide III region was dominated by the Y7a′ mode of tyrosine. Introduction of myricetin resulted in a significant increase in the intensity of the tyrosine band at 1615 cm^{-1}, consistent with reduced exposure to the solvent environment [68].

3.4. Myricetin's intrinsic fluorescence

A significant binding interaction might affect the intrinsic fluorescent properties of myricetin; therefore, the fluorescence spectra of myricetin were monitored before and after the addition of each peptide. In aqueous solutions, myricetin is weakly fluorescent and has two fluorescence maxima at 481 and 531 nm (Fig. 5). As the concentration of myricetin increases, the intensity at 531 nm increases proportionally, whereas the intensity at 481 nm remains essentially unchanged (data not shown). Similar behavior has been observed for the flavonoid quercetin [71]; the two maxima were attributed to the enol and keto photo-tautomers, respectively. Quercetin exhibits greater keto-enol photo-tautomerism at higher concentrations, where formation of aggregates is expected, suggesting that photo-tautomerism is facilitated by intermolecular transfer of protons [71]. Thus, it is likely that the two fluorescence maxima of myricetin can also be assigned to enol and keto photo-tautomers of myricetin. At 25 μM, the fluorescence intensity of myricetin at 481 nm is overwhelmed by the relatively higher fluorescence intensity at 531 nm, which may be assigned to keto photo-tautomers resulting from myricetin's self-association. To better visualize the fluorescence properties of monomeric myricetin at 481 nm, 10 μM myricetin was used. The fluorescence spectra of 10 μM myricetin may be deconvoluted into three components, which are located at 481, 531 and 573 nm, respectively. The fluorescence intensity of myricetin at 481 nm significantly decreased with the addition of 30 μM Aβ(25–40) or Aβ(1–42) (Fig. 5, Table 1). The addition of Aβ(1–16) did not result in a significant decrease in myricetin's fluorescence at 481 nm (Fig. 5). Moreover, the fluorescence intensity of myricetin at both 531 and 573 nm also decreased significantly with the addition of Aβ(25–40), whereas these peaks were not significantly affected by the addition of Aβ(1–42) and Aβ(1–16) (Table 1).

4. Discussion and conclusions

ThT fluorescence assays showed that the polyphenolic flavonoid, myricetin, fully inhibited Aβ(1–42) and the hydrophobic fragment, Aβ(25–40), from forming amyloid (cross β-sheet) structures (Fig. 1). However, some small molecules displace ThT rather than inhibiting amyloid formation. Cross β-sheet structures have similar CD spectra to β-sheet proteins; therefore, CD was employed to confirm that myricetin fully inhibited β-sheet (amyloid) formation (Fig. 2). Deep-UVRR spectroscopic studies of Aβ(1–42) and Aβ(1–16) indicated that introduction of myricetin altered the environment of the aromatic residues, suggesting that myricetin may be interacting with these residues. Interestingly, Aβ(25–40) has no aromatic residues; therefore, additional interactions with the hydrophobic region may include hydrogen bonding with the backbone or charged lysine residue and hydrophobic interactions. A small but reproducible reduction in the mean residue ellipticity at 197 nm in the CD spectra of Aβ(1–42) and Aβ(25–40) upon introduction of myricetin likely indicates a small change in the secondary structure of these peptides; however, a significant conformational change in a small fraction of the bulk population cannot be ruled out. In combination, these data suggest that myricetin interacts with the aromatic residues of Aβ and induces a small conformational change in the hydrophobic region of the peptide. A reduction in the negative intensity at 197 nm could potentially be attributed to a reduction in the relative amount of β-strand structure [46] or an increase in the amorphous structure of the peptide [47]. Either scenario could result in a reduced propensity to form amyloid structure.

A relatively small, but reproducible, shift in the amide I band of Aβ(1–42) was observed in the presence of myricetin. Surprisingly, no other changes in the amide regions were observed. The amide III mode is directly overlapped with the Y7a′ mode. Thus, any changes in this region could be obscured by tyrosine. The amide I and III bands increased slightly in the UVRR spectrum of Aβ(25–40) when myricetin was introduced, but again the changes are small and difficult to assign. In combination, the CD and UVRR data suggest that the secondary structure of the bulk portion of the peptide remains unchanged. Interestingly, significant increases in intensity were observed for the aromatic bands at 1208, 1585 and 1610 cm^{-1}. The bands at 1208 (F7a + Y7a) and 1610 (F8b + Y8a) cm^{-1} are a mixture of tyrosine and weaker phenylalanine modes. The band at 1585 cm^{-1} (F8a) is attributed solely to phenylalanine. Based on these data it can be suggested that myricetin interacts with one or more phenylalanine residues in Aβ(1–42) and possibly the single tyrosine residue.

The CD difference spectrum of the hydrophilic peptide Aβ(1–16) shows a significant decrease in the ellipticity just above 210 nm (Fig. 3, inset). It should be noted that no significant change was observed in this region for the full-length peptide. Both tyrosine and phenylalanine contribute to the CD spectrum in this region [50,49]. The UVRR difference spectrum of Aβ(1–16) shows a strong increase caused by myricetin in the intensity of the tyrosine band at 1615 cm^{-1}. Taken together the CD and UVRR data are consistent with myricetin-induced changes in the environment surrounding the aromatic residues. Although interactions with phenylalanine cannot be ruled out, the UVRR spectrum of Aβ(1–16) indicates changes caused by myricetin in the environment surrounding tyrosine. Furthermore, Aβ(1–16) does not appear to undergo a conformational change upon introduction of myricetin.

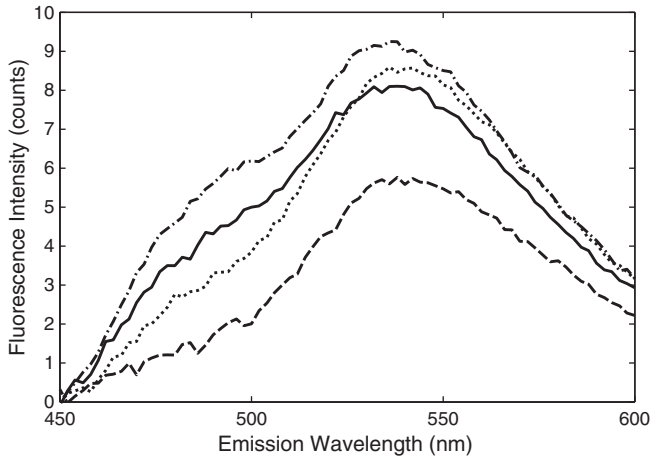

Fig. 5. Fluorescence spectra of (·—·—) 10 μM myricetin, (— —) 10 μM myricetin with 30 μM Aβ(25–40), (—) 10 μM myricetin with 30 μM Aβ(1–16) and (· · ·) 10 μM myricetin with 30 μM Aβ(1–42) in pH 7.4 phosphate buffer (λ_{Ex} = 380 nm).

Table 1
Fitted peak areas from deconvoluted fluorescence spectra of 10 μM myricetin by itself and with Aβ(25–40), Aβ(1–16) and Aβ(1–42).

Peak center (nm)	10 μM myricetin (10 replicates)	Aβ(25–40)/ 10 μM myricetin (7 replicates)	Aβ(1–16)/ 10 μM myricetin (11 replicates)	Aβ(1–42)/ 10 μM myricetin (3 replicates)
481 ± 2	59 ± 8	15 ± 2*	50 ± 20	31 ± 2*
531 ± 2	230 ± 20	140 ± 30*	210 ± 40	210 ± 10
573 ± 1	140 ± 20	110 ± 20*	120 ± 20	133 ± 7

*Significant difference compared to myricetin alone, as determined by the extended *t* test at a 95% significant level.

Other polyphenols have been shown to interact with disordered proline rich salivary proteins through hydrophobic and backbone interactions [72]. The hydrophobic fragment Aβ(25–40) contains no aromatic residues and is more soluble than the more frequently studied Aβ(25–35), making it an ideal candidate to determine whether hydrophobic or backbone interactions can play a role in the anti-amyloidogenic behavior of myricetin. ThT fluorescence assays established that Aβ(25–40) was able to form an amyloid structure and that myricetin inhibited this process. Similar to the full-length peptide, the CD difference spectrum of Aβ(25–40) (Fig. 1, inset) also shows a myricetin-induced decrease in the intensity of the mean residue ellipticity at 197 nm. However, unlike the full-length peptide, small changes were observed in the amide I and III regions, in comparison to the amide S band, of the UVRR spectrum of Aβ(25–40), which is consistent with a small increase in the PPII content.

These data suggest that aromatic and non-aromatic (hydrophobic, charged residue or backbone) interactions contribute to myricetin's anti-amyloidogenic effect. What is also interesting is that each peptide appears to interact with myricetin in a slightly different manner, Aβ(1–16) through aromatic interactions with tyrosine, Aβ(25–40) through hydrophobic or backbone interactions and Aβ(1–42) through aromatic interactions with the phenylalanine residues and non-aromatic interactions.

Acknowledgements

The authors thank Dr. Michael Henzl and Dr. Anmin Tan for help with the CD measurements. The authors also thank the University of Missouri Research Council and University of Missouri Research Board for funding.

References

[1] C.L. Masters, R. Cappai, K.J. Barnham, V.L. Villemagne, Molecular mechanisms for Alzheimer's disease: implications for neuroimaging and therapeutics, J. Neurochem. 97 (2006) 1700–1725.
[2] L.-F. Lue, Y.-M. Kuo, A.E. Roher, L. Brachova, Y. Shen, L. Sue, T. Beach, J.H. Kurth, R.E. Rydel, J. Rogers, Soluble amyloid β peptide concentration as a predictor of synaptic change in Alzheimer's disease, Am. J. Pathol. 155 (1999) 853–862.
[3] C.A. McLean, R.A. Cherny, F.W. Fraser, S.J. Fuller, M.J. Smith, K. Beyreuther, A.I. Bush, C.L. Masters, Soluble pool of Aβ amyloid as a determinant of severity of neurodegeneration in Alzheimer's disease, Ann. Neurol. 46 (1999) 860–866.
[4] M.M. Husain, K. Trevino, H. Siddique, S.M. McClintock, Present and prospective clinical therapeutic regimens for Alzheimer's disease, Neuropsychiatr. Dis. Treat. 4 (2008) 765–777.
[5] N.C. Inestrosa, M.C. Dinamarca, A. Alvarez, Amyloid–cholinesterase interactions. Implications for Alzheimer's disease, FEBS J. 275 (2008) 625–632.
[6] T. Heinen-Kammerer, H. Rulhoff, S. Nelles, R. Rychlik, Added therapeutic value of memantine in the treatment of moderate to severe Alzheimer's disease, Clin. Drug Investig. 26 (2006) 303–314.
[7] M. Asai, C. Hattori, N. Iwata, T.C. Saido, N. Sasagawa, B. Szabo, Y. Hashimoto, K. Maruyama, S. Tanuma, Y. Kiso, S. Ishiura, The novel β-secretase inhibitor KMI-429 reduces amyloid beta peptide production in amyloid precursor protein transgenic and wild-type mice, J. Neurochem. 96 (2006) 533–540.
[8] G.K. Wilcock, S.E. Black, S.B. Hendrix, K.H. Zavitz, E.A. Swabb, M.A. Laughlin, Efficacy and safety of tarenflurbil in mild to moderate Alzheimer's disease: a randomised phase II trial, Lancet neurology 7 (2008) 483–493.
[9] J. Walter, C. Kaether, H. Steiner, C. Haass, The cell biology of Alzheimer's disease: uncovering the secrets of secretases, Curr. Opin. Neurobiol. 11 (2001) 585–590.
[10] D. Schenk, R. Barbour, W. Dunn, G. Gordon, H. Grajeda, T. Guido, K. Hu, J. Huang, K. Johnson-Wood, K. Khan, D. Kholodenko, M. Lee, Z. Liao, I. Lieberburg, R. Motter, L. Mutter, F. Soriano, G. Shopp, N. Vasquez, C. Vandevert, S. Walker, M. Wogulis, T. Yednock, D. Games, P. Seubert, Immunization with amyloid-β attenuates Alzheimer-disease-like pathology in the PDAPP mouse, Nature 400 (1999) 173–177.
[11] J.-M. Orgogozo, S. Gilman, J.-F. Dartigues, B. Laurent, M. Puel, L.C. Kirby, P. Jouanny, B. Dubois, L. Eisner, S. Flitman, B.F. Michel, M. Boada, A. Frank, C. Hock, Subacute meningoencephalitis in a subset of patients with AD after Aβ42 immunization, Neurology 61 (2003) 46–54.
[12] K. Samson, 'Passive' Alzheimer vaccine gets accelerated phase 3 start, Neurology Today 7 (2007) 15–16.
[13] J.O. Rinne, D.J. Brooks, M.N. Rossor, N.C. Fox, R. Bullock, W.E. Klunk, C.A. Mathis, K. Blennow, J. Barakos, A.A. Okello, S.R.M. de Liano, E. Liu, M. Koller, K.M. Gregg, D. Schenk, R. Black, M. Grundman, 11C-PiB PET assessment of change in fibrillar amyloid-β load in patients with Alzheimer's disease treated with bapineuzumab: a phase 2, double-blind, placebo-controlled, ascending-dose study, Lancet Neurol. 9 (2010) 363–372.
[14] T.E. Golde, Disease modifying therapy for AD? J. Neurochem. 99 (2006) 689–707.
[15] C. Féart, C. Samieri, P. Barberger-Gateau, Mediterranean diet and cognitive function in older adults, Curr. Opin. Clin. Nutr. 13 (2010) 14–18.
[16] S. Bastianetto, R. Quirion, Natural extracts as possible protective agents of brain aging, Neurobiol. Aging 23 (2002) 891–897.
[17] G.P. Lim, T. Chu, F. Yang, W. Beech, S.A. Frautschy, G.M. Cole, The curry spice curcumin reduces oxidative damage and amyloid pathology in an Alzheimer transgenic mouse, J. Neurosci. 21 (2001) 8370–8377.
[18] Q. Wang, A. Simonyi, W.L. Li, B.A. Sisk, R.L. Miller, R.S. MacDonald, D.E. Lubahn, G.Y. Sun, A.Y. Sun, Dietary grape supplement ameliorates cerebral ischemia-induced neuronal death in gerbils, Mol. Nutr. Food Res. 49 (2005) 443–451.
[19] Q. Wang, A.Y. Sun, A. Simonyi, M.D. Jensen, P.B. Shelat, G.E. Rottinghaus, R.S. MacDonald, D.K. Miller, D.E. Lubahn, G.A. Weisman, G.Y. Sun, Neuroprotective mechanisms of curcumin against cerebral ischemia-induced neuronal apoptosis and behavioral deficits, J. Neurosci. Res. 82 (2005) 138–148.
[20] M. Necula, R. Kayed, S. Milton, C.G. Glabe, Small molecule inhibitors of aggregation indicate that amyloid β oligomerization and fibrillization pathways are independent and distinct, J. Biol. Chem. 282 (2007) 10311–10324.
[21] H. Levine III, Small molecule inhibitors of Aβ assembly, Amyloid 14 (2007) 185–197.
[22] T. Bandiera, J. Lansen, C. Post, M. Varasi, Inhibitors of Aβ peptide aggregation as potential anti-Alzheimer agents, Curr. Med. Chem. 4 (1997) 159–170.
[23] F.S. Yang, G.P. Lim, A.N. Begum, O.J. Ubeda, M.R. Simmons, S.S. Ambegaokar, P.P. Chen, R. Kayed, C.G. Glabe, S.A. Frautschy, G.M. Cole, Curcumin inhibits formation of amyloid beta oligomers and fibrils, binds plaques, and reduces amyloid *in vivo*, J. Biol. Chem. 280 (2005) 5892–5901.
[24] M. Pappolla, P. Bozner, C. Soto, H.Y. Shao, N.K. Robakis, M. Zagorski, B. Frangione, J. Ghiso, Inhibition of Alzheimer β-fibrillogenesis by melatonin, J. Biol. Chem. 273 (1998) 7185–7188.
[25] T. Tomiyama, S. Asano, Y. Suwa, T. Morita, K. Kataoka, H. Mori, N. Endo, Rifampicin prevents the aggregation and neurotoxicity of amyloid-β protein *in-vitro*, Biochem. Biophys. Res. Commun. 204 (1994) 76–83.
[26] J. McLaurin, R. Golomb, A. Jurewicz, J.P. Antel, P.E. Fraser, Inositol stereoisomers stabilize an oligomeric aggregate of Alzheimer amyloid β peptide and inhibit Aβ-induced toxicity, J. Biol. Chem. 275 (2000) 18495–18502.
[27] P. Marambaud, H. Zhao, P. Davies, Resveratrol promotes clearance of Alzheimer's disease amyloid-β peptides, J. Biol. Chem. 280 (2005) 37377–37382.
[28] J.B. Hoppe, R.L. Frozza, A.P. Horn, R.A. Comiran, A. Bernardi, M.M. Campos, A.M.O. Battastini, C. Salbego, Amyloid-β neurotoxicity in organotypic culture is attenuated by melatonin: involvement of GSK-3β, tau and neuroinflammation, J. Pineal Res. 48 (2010) 230–238.
[29] T. Tomiyama, H. Kaneko, K. Kataoka, S. Asano, N. Endo, Rifampicin inhibits the toxicity of pre-aggregated amyloid peptides by binding to peptide fibrils and preventing amyloid-cell interaction, Biochem. J. 322 (1997) 859–865.
[30] K. Ono, Y. Yoshiike, A. Takashima, K. Hasegawa, H. Naiki, M. Yamada, Potent anti-amyloidogenic and fibril-destabilizing effects of polyphenols *in vitro*: implications for the prevention and therapeutics of Alzheimer's disease, J. Neurochem. 87 (2003) 172–181.
[31] H. Kim, B.S. Park, K.G. Lee, C.Y. Choi, S.S. Jang, Y.H. Kim, S.E. Lee, Effects of naturally occurring compounds on fibril formation and oxidative stress of β-amyloid, J. Agric. Food Chem. 53 (2005) 8537–8541.
[32] H. Onozuka, A. Nakajima, K. Matsuzaki, R.W. Shin, K. Ogino, D. Saigusa, N. Tetsu, A. Yokosuka, Y. Sashida, Y. Mimaki, T. Yamakuni, Y. Ohizumi, Nobiletin, a citrus flavonoid, improves memory impairment and Aβ pathology in a transgenic mouse model of Alzheimer's disease, J. Pharmacol. Exp. Ther. 326 (2008) 739–744.
[33] A.M. Haque, M. Hashimoto, M. Katakura, Y. Hara, O. Shido, Green tea catechins prevent cognitive deficits caused by Aβ1–40 in rats, J. Nutr. Biochem. 19 (2008) 619–626.
[34] S. Burda, W. Oleszek, Antioxidant and antiradical activities of flavonoids, J. Agric. Food Chem. 49 (2001) 2774–2779.
[35] H.A. Scheidt, A. Pampel, L. Nissler, R. Gebhardt, D. Huster, Investigation of the membrane localization and distribution of flavonoids by high-resolution magic angle spinning NMR spectroscopy, Biochim. Biophys. Acta 1663 (2004) 97–107.
[36] T. Hamaguchi, K. Ono, A. Murase, M. Yamada, Phenolic compounds prevent Alzheimer's pathology through different effects on the amyloid-β aggregation pathway, Am. J. Pathol. 175 (2009) 2557–2565.
[37] M. Hirohata, K. Hasegawa, S. Tsutsumi-Yasuhara, Y. Ohhashi, T. Ookoshi, K. Ono, M. Yamada, H. Naiki, The anti-amyloidogenic effect is exerted against Alzheimer's β-amyloid fibrils in vitro by preferential and reversible binding of flavonoids to the amyloid fibril structure, Biochemistry 46 (2007) 1888–1899.
[38] Y. Shimmyo, T. Kihara, A. Akaike, T. Niidome, H. Sugimoto, Multifunction of myricetin on Aβ: neuroprotection via a conformational change of Aβ and reduction of Aβ via the interference of secretases, J. Neurosci. Res. 86 (2008) 368–377.
[39] T. Richard, X. Vitrac, J.M. Merillon, J.P. Monti, Role of peptide primary sequence in polyphenol–protein recognition: an example with neurotensin, Biochim. Biophys. Acta-Gen. Subj. 1726 (2005) 238–243.
[40] N.J. Murray, M.P. Williamson, T.H. Lilley, E. Haslam, Study of the interaction between salivary proline-rich proteins and a polyphenol by ^{1}H-NMR spectroscopy, Eur. J. Biochem. 219 (1994) 923–935.
[41] D.B. Teplow, Preparation of amyloid beta-protein for structural and functional studies, Methods Enzymol. 413 (2006) 20–33.
[42] L.J. Saidel, A.R. Goldfarb, S. Waldman, The absorption spectra of amino acids in the region two hundred to two hundred and thirty millimicrons, J. Biol. Chem. 197 (1952) 285–291.

[43] M.L. Tiffany, S. Krimm, Circular dichroism of poly-L-proline in an unordered conformation, Biopolymers 6 (1968) 1767–1770.
[44] M.L. Tiffany, S. Krimm, Extended conformations of polypeptides and proteins in urea and guanidine hydrochloride, Biopolymers 12 (1973) 575–587.
[45] M.L. Tiffany, S. Krimm, New chain conformations of poly(glutamic acid) and polylysine, Biopolymers 6 (1968) 1379–1382.
[46] B.W. Chellgren, T.P. Creamer, Short sequences of non-proline residues can adopt the polyproline II helical conformation, Biochemistry 43 (2004) 5864–5869.
[47] M.L. Tiffany, S. Krimm, Circular dichroism of random polypeptide chain, Biopolymers 8 (1969) 347–359.
[48] J. Danielsson, J. Jarvet, P. Damberg, A. Graslund, The Alzheimer β-peptide shows temperature-dependent transitions between left-handed 3_1-helix, β-strand and random coil secondary structures, FEBS J. 272 (2005) 3938–3949.
[49] E. Peggion, A. Cosani, M. Terbojev, L. Romaninj, Random coil-β-form transition of poly-L-lysine - Evidence for formation of α-helical structure during transition, J. Chem. Soc.-Chem. Commun. (1974) 314–316.
[50] A. Chakrabartty, T. Kortemme, S. Padmanabhan, R.L. Baldwin, Aromatic side-chain contribution to far-ultraviolet circular dichroism of helical peptides and its effect on measurement of helix propensities, Biochemistry 32 (1993) 5560–5565.
[51] Z. Chi, X.G. Chen, J.S.W. Holtz, S.A. Asher, UV resonance Raman-selective amide vibrational enhancement: quantitative methodology for determining protein secondary structure, Biochemistry 37 (1998) 2854–2864.
[52] R.A. Copeland, T.G. Spiro, Secondary structure determination in proteins from deep (192–223 nm) ultraviolet Raman-spectroscopy, Biochemistry 26 (1987) 2134–2139.
[53] R.D. JiJi, G. Balakrishnan, Y. Hu, T.G. Spiro, Intermediacy of poly(L-proline) II and β-strand conformations in poly(L-lysine) β-sheet formation probed by temperature-jump/UV resonance Raman spectroscopy, Biochemistry 45 (2006) 34–41.
[54] Y. Wang, R. Purrello, S. Georgiou, T.G. Spiro, UVRR spectroscopy of the peptide-bond. 2. Carbonyl H-bond effects on the ground-state and excited-state structures of *N*-methylacetamide, J. Am. Chem. Soc. 113 (1991) 6368–6377.
[55] C.J. Barrow, A. Yasuda, P.T.M. Kenny, M.G. Zagorski, Solution conformations and aggregational properties of synthetic amyloid β-peptides of Alzheimers-disease—analysis of circular-dichroism spectra, J. Mol. Biol. 225 (1992) 1075–1093.
[56] L.A. Popova, R. Kodali, R. Wetzel, I.K. Lednev, Structural variations in the cross-beta core of amyloid beta fibrils revealed by deep UV resonance Raman spectroscopy, J. Am. Chem. Soc. 132 (2010) 6324–6328.
[57] Z. Ye, K.C. French, L.A. Popova, I.K. Lednev, M.M. Lopez, G.I. Makhatadze, Mechanism of fibril formation by a 39-residue peptide (PAPf39) from human prostatic acidic phosphatase, Biochemistry 48 (2009) 11582–11591.
[58] M. Xu, V.V. Ermolenkov, V.N. Uversky, I.K. Lednev, Hen egg white lysozyme fibrillation: a deep-UV resonance Raman spectroscopic study, J. Biophotonics 1 (2008) 215–229.
[59] M. Xu, V.A. Shashilov, V.V. Ermolenkov, L. Fredriksen, D. Zagorevski, I.K. Lednev, The first step of hen egg white lysozyme fibrillation, irreversible partial unfolding, is a two-state transition, Protein Sci. 16 (2007) 815–832.
[60] M. Xu, V.V. Ermolenkov, W. He, V.N. Uversky, L. Fredriksen, I.K. Lednev, Lysozyme fibrillation: deep UV Raman spectroscopic characterization of protein structural transformation, Biopolymers 79 (2005) 58–61.
[61] Y. Wang, S. Petty, A. Trojanowski, K. Knee, D. Goulet, I. Mukerji, J. King, Formation of amyloid fibrils in vitro from partially unfolded intermediates of human gammaC-crystallin, Invest. Ophth. Vis. Sci. 51 (2010) 672–678.
[62] S.H. Song, S.A. Asher, UV resonance Raman studies of peptide conformation in poly(L-lysine), poly(L-glutamic acid), and model complexes—the basis for protein secondary structure determinations, J. Am. Chem. Soc. 111 (1989) 4295–4305.
[63] Y. Wang, R. Purrello, T. Jordan, T.G. Spiro, UVRR spectroscopy of the peptide bond. 1. Amide S, a nonhelical structure marker, is a CαH bending mode, J. Am. Chem. Soc. 113 (1991) 6359–6368.
[64] C.Y. Huang, G. Balakrishnan, T.G. Spiro, Protein secondary structure from deep-UV resonance Raman spectroscopy, J. Raman Spectrosc. 37 (2006) 277–282.
[65] A.V. Mikhonin, N.S. Myshakina, S.V. Bykov, S.A. Asher, UV resonance Raman determination of polyproline II, extended 2.5_1-helix, and β-sheet psi angle energy landscape in poly-L-lysine and poly-L-glutamic acid, J. Am. Chem. Soc. 127 (2005) 7712–7720.
[66] A.V. Mikhonin, S.V. Bykov, N.S. Myshakina, S.A. Asher, Peptide secondary structure folding reaction coordinate: correlation between UV Raman amide III frequency, Psi Ramachandran angle, and hydrogen bonding, J. Phys. Chem. B 110 (2006) 1928–1943.
[67] S.A. Asher, A. Ianoul, G. Mix, M.N. Boyden, A. Karnoup, M. Diem, R. Schweitzer-Stenner, Dihedral psi angle dependence of the amide III vibration: a uniquely sensitive UV resonance Raman secondary structural probe, J. Am. Chem. Soc. 123 (2001) 11775–11781.
[68] R.P. Rava, T.G. Spiro, Ultraviolet resonance Raman spectra of insulin and alpha-lactalbumin with 218- and 200-nm laser excitation, Biochemistry 24 (1985) 1861–1865.
[69] J.C. Austin, T. Jordan, T.G. Spiro, Ultraviolet resonance Raman studies of proteins and related model compounds, in: R.J.H. Clark, R.E. Hester (Eds.), Biomolecular Spectroscopy, Wiley & Sons Ltd., New York, 1993, pp. 55–127.
[70] G. Socrates, Infrared and Raman Characteristic Group Frequencies, Third ed. John Wiley & Sons, Ltd., Chichester, 2001.
[71] G.J. Smith, K.R. Markham, Tautomerism of flavonol glucosides: relevance to plant UV protection and flower colour, J. Photochem. Photobiol. A Chem. 118 (1998) 99–105.
[72] T. Richard, D. Lefeuvre, A. Descendit, S. Quideau, J.P. Monti, Recognition characters in peptide–polyphenol complex formation, Biochim. Biophys. Acta-Gen. Subj. 1760 (2006) 951–958.